Supplementary Information

From 2D to 3D Plasmonic Periodic Heterostructures: How Plasmon Resonance Influences on Photocatalytic Degradation

Section SI. Characteration of Au/Ag-TiO_2 Heterostructure

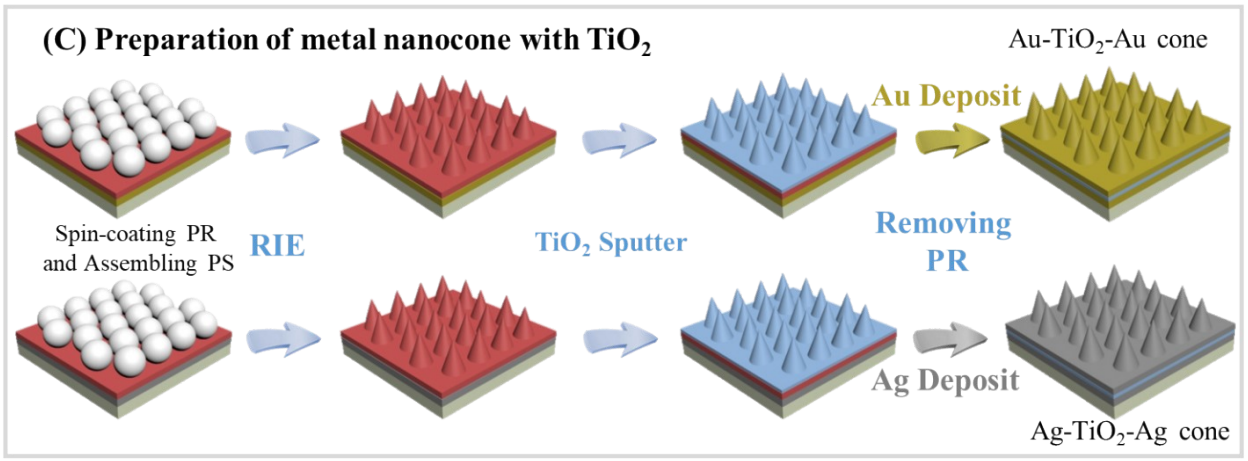
(C) Preparation of metal nanocone with TiO2
Au-TiO2-Au cone
Au Deposit
Spin-coating PR
and Assembling PS
RIE
TiO2 Sputter
Removing
PR
Ag Deposit
Ag-TiO2-Ag cone

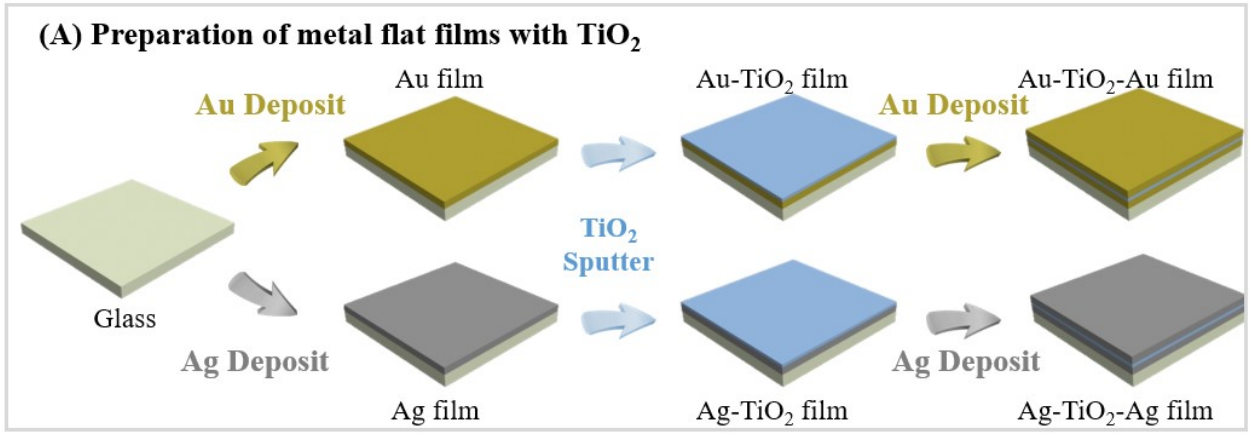
(A) Preparation of metal flat films with TiO2
Au film
Au-TiO2 film
Au-TiO2-Au film
Au Deposit
Au Deposit
TiO2
Sputter
Glass
Ag Deposit
Ag Deposit
Ag film
Ag-TiO2 film
Ag-TiO2-Ag film

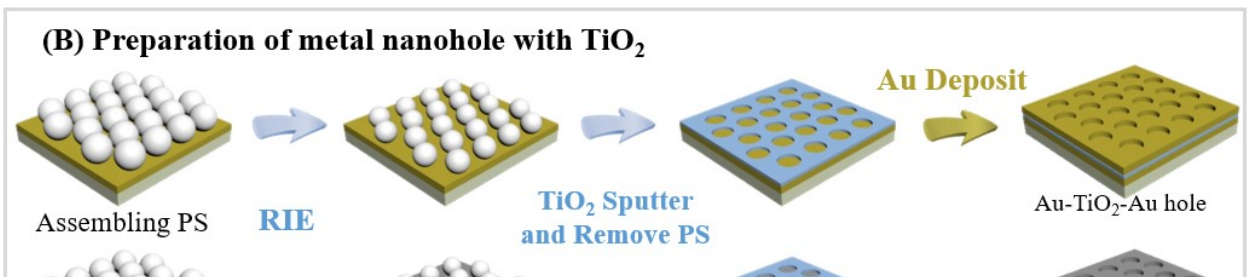
(B) Preparation of metal nanohole with TiO2
Au Deposit
Assembling PS
RIE
TiO2 Sputter
and Remove PS
Au-TiO2-Au hole

Figure S1. Schematic illustration of preparation of (A) Au/Ag flat films with TiO_2, (B) Au/Ag nanohole with TiO_2, and (C) Au/Ag nanocone with TiO_2.

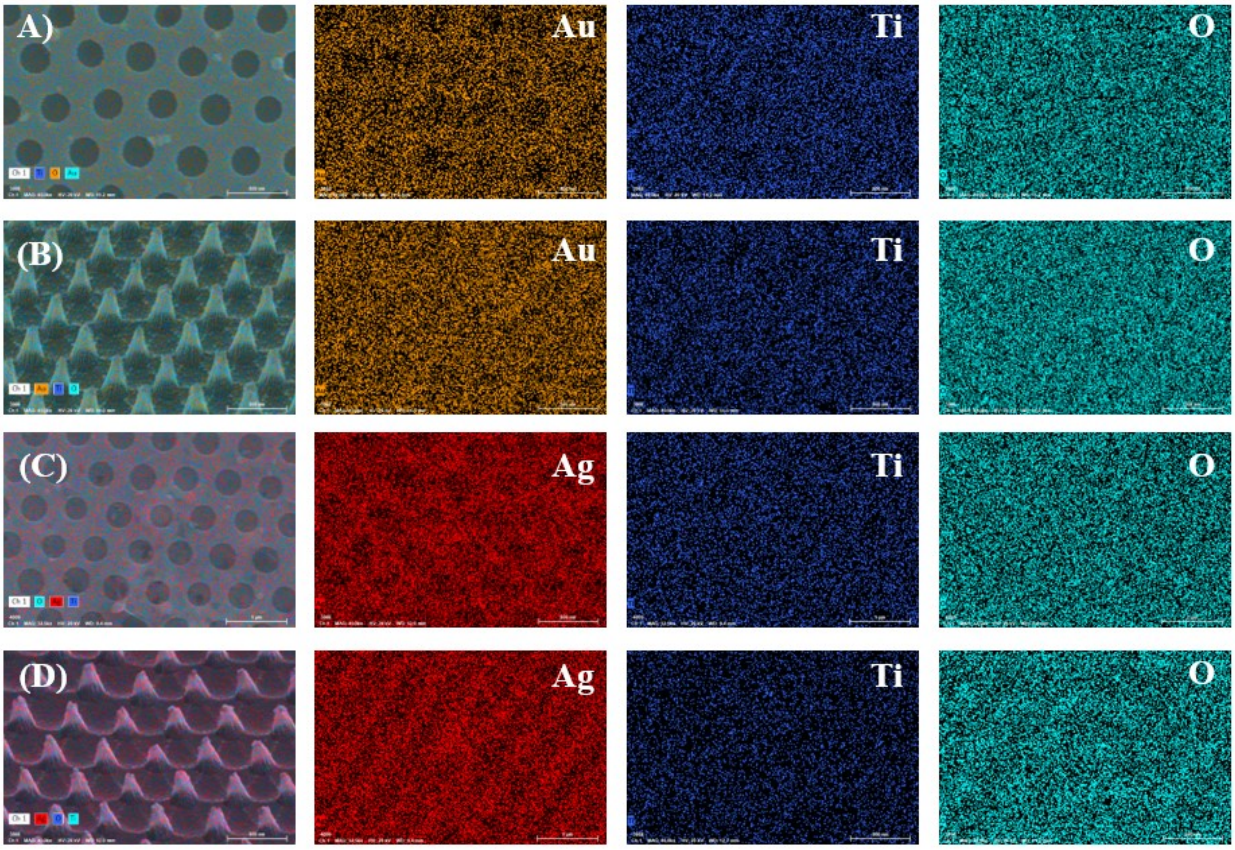

Figure S2. EDS pictures of (A) Au-TiO_2-Au hole, (B) Au-TiO_2-Au cone, (C) Ag-TiO_2-Ag hole and (D) Ag-TiO_2-Ag cone.

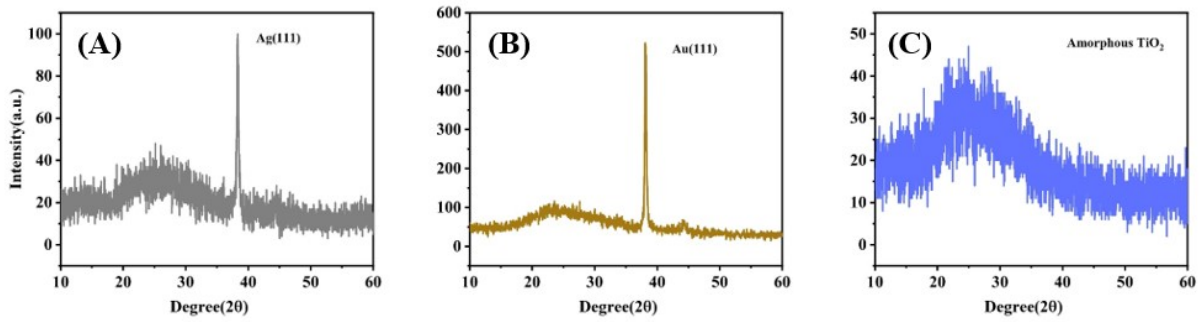

Figure S3. X-Ray diffraction (XRD) images of (A) Ag(111), (B) Au(111) and (C) amorphous TiO_2.

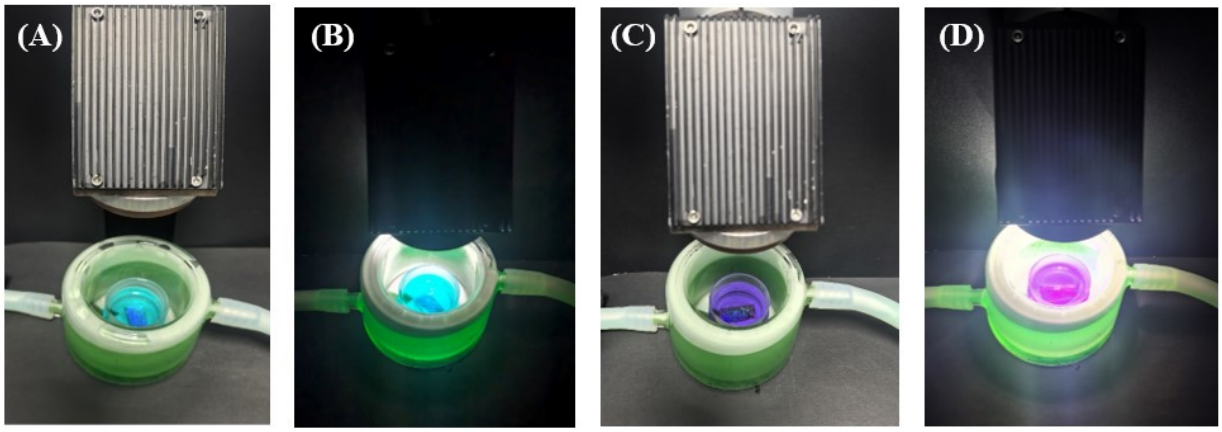

Figure S4. Photograph showing the degradation of organic dyes under xenon lamp irradiation with same size of (A) Ag–TiO_2–Ag hole in MB with light off, (B) Ag–TiO_2–Ag hole in MB with light on, (C) Au–TiO_2–Au hole in CV with light off and (D) Au–TiO_2–Au hole in CV with light on.

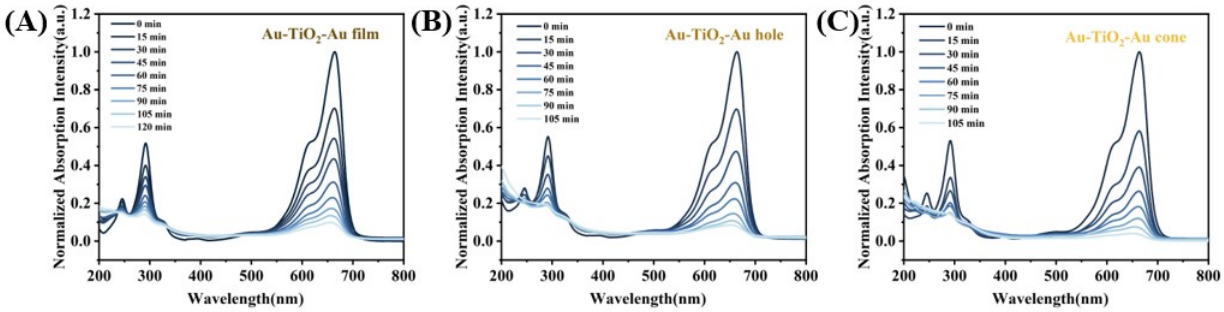

Figure S5. Normalized UV absorption spectra of Methylene Blue (MB) at different light exposure times of (A) Au–TiO_2–Au film, (B) Au–TiO_2–Au hole, (C) Au–TiO_2–Au cone.

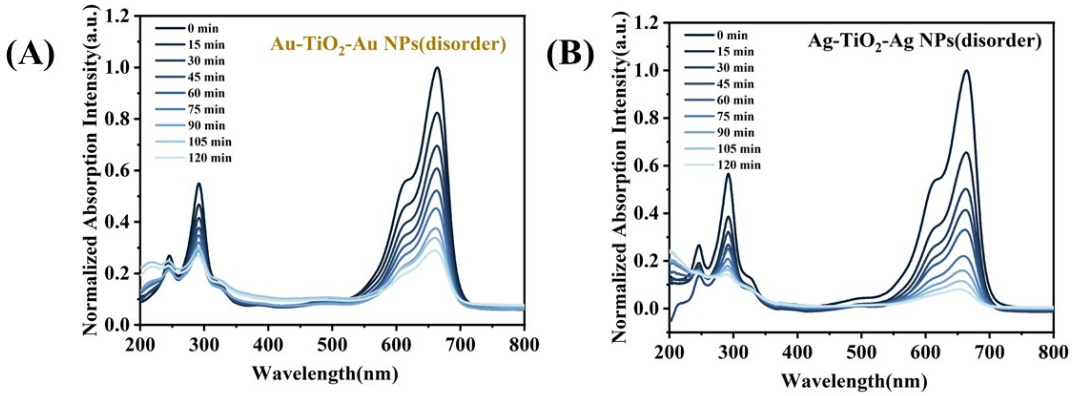

Figure S6. Normalized UV absorption spectra of Methylene Blue (MB) at different light exposure times of (A) Au–TiO_2–disorder Au NPs and (B) Ag–TiO_2–disorder Ag NPs.

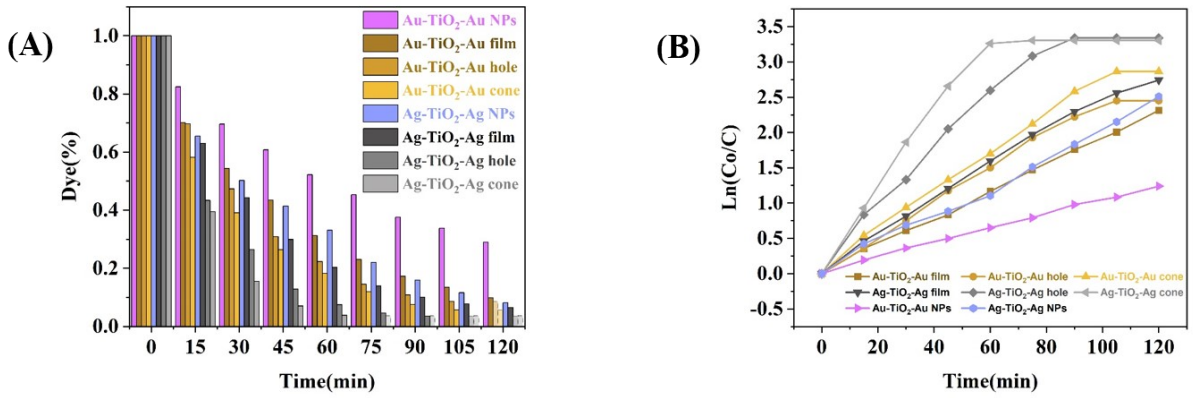

Figure S7. (A) Degradation Efficiency of MB with Different Structures,（B）Comparison of Reaction Rates for Different Structures.

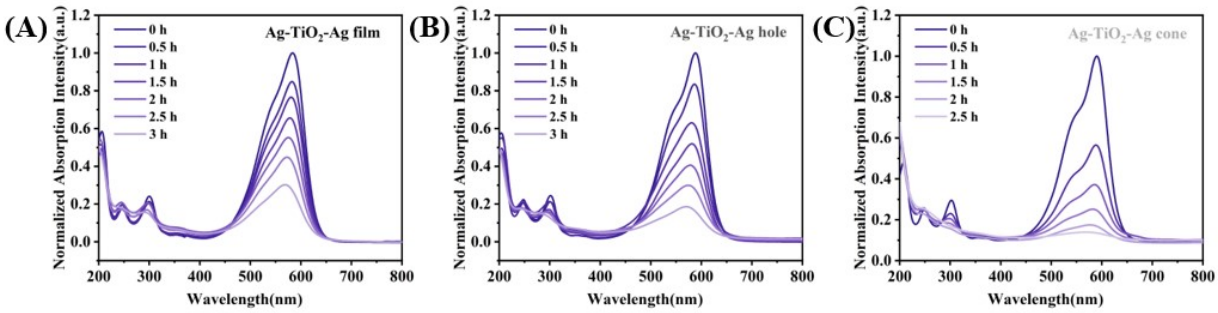

Figure S8. Normalized UV absorption spectra of Crystal violet (CV) at different light exposure times of (A) Ag–TiO_2–Ag film, (B) Ag–TiO_2–Ag hole, (C) Ag–TiO_2–Ag cone.

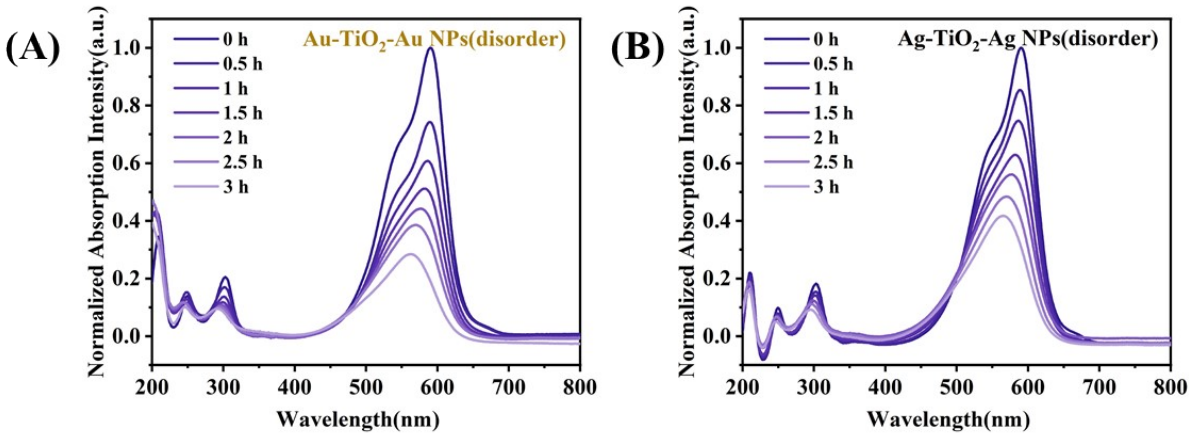

Figure S9. Normalized UV absorption spectra of Crystal violet (CV) at different light exposure times of (A) Au–TiO_2–disorder Au NPs and (B) Ag–TiO_2–disorder Ag NPs.

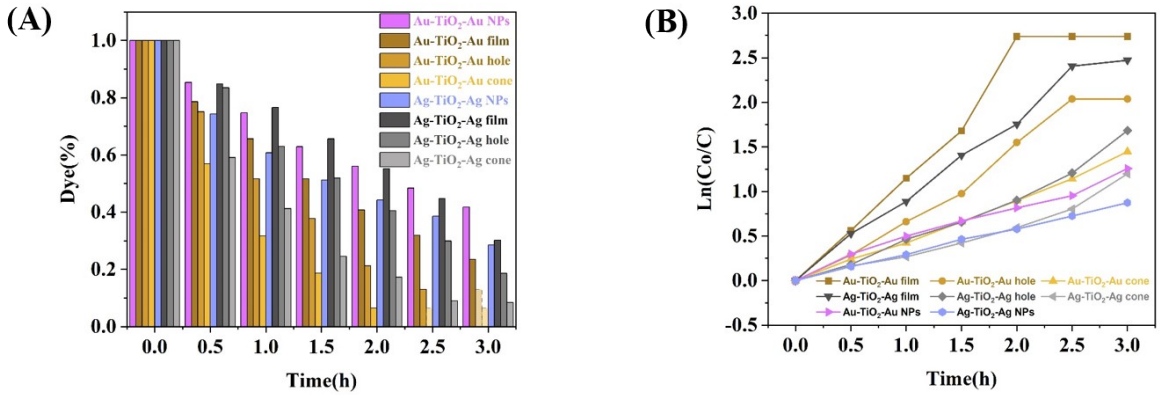

Figure S10. (A) Degradation Efficiency of CV with Different Structures,（B）Comparison of Reaction Rates for Different Structures.

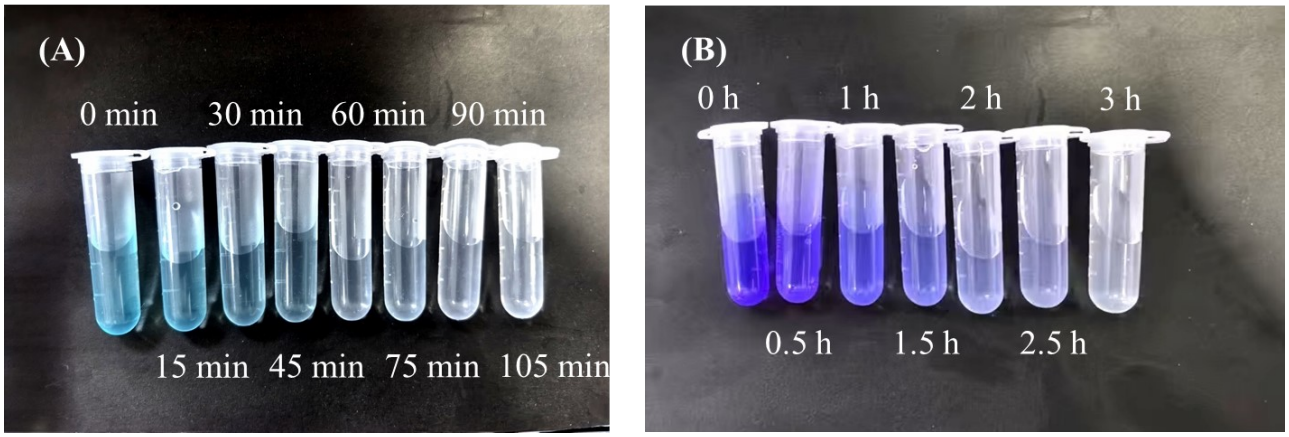

Figure S11. Photograph showing the degradation of organic dyes under xenon lamp irradiation with different times of (A) MB and (B) CV.

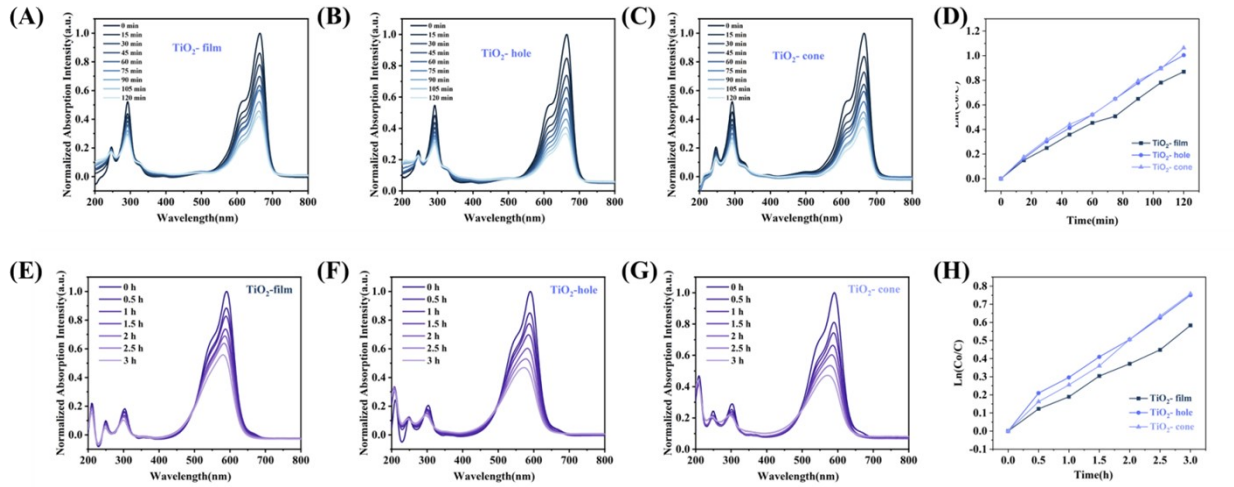

Figure S12. Normalized UV absorption spectra of MB at different light exposure times of (A) Ag+TiO_2+Ag film, (B) Ag+TiO_2+Ag hole, (C) Ag+TiO_2+Ag cone. Normalized UV absorption spectra of CV at different light exposure times of (E) TiO_2 film, (F) TiO_2 hole, (G) TiO_2 cone. Comparison of Reaction Rates for Different Structures (D) of MB and (H) of CV.

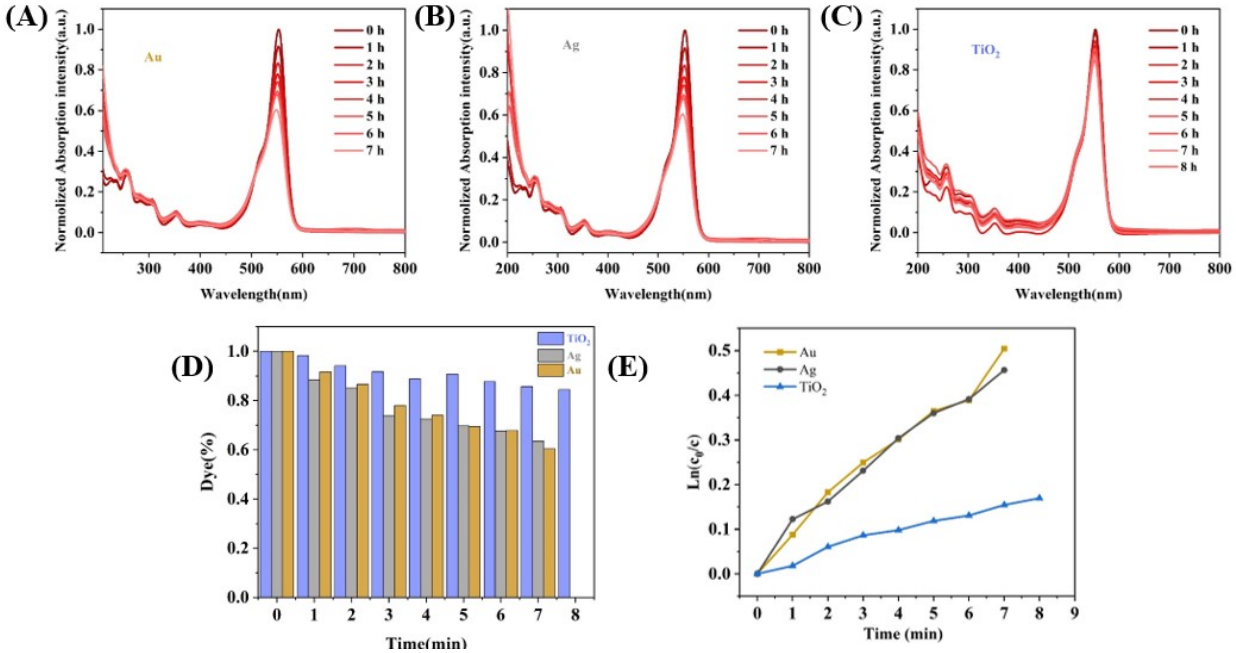

Figure S13. Normalized UV absorption spectra of RhB at different light exposure times of (A) TiO_2, (B) Ag, (C) Au. (D) Degradation efficiency of RhB with different structures. (E) Comparison of reaction rates for different structures.

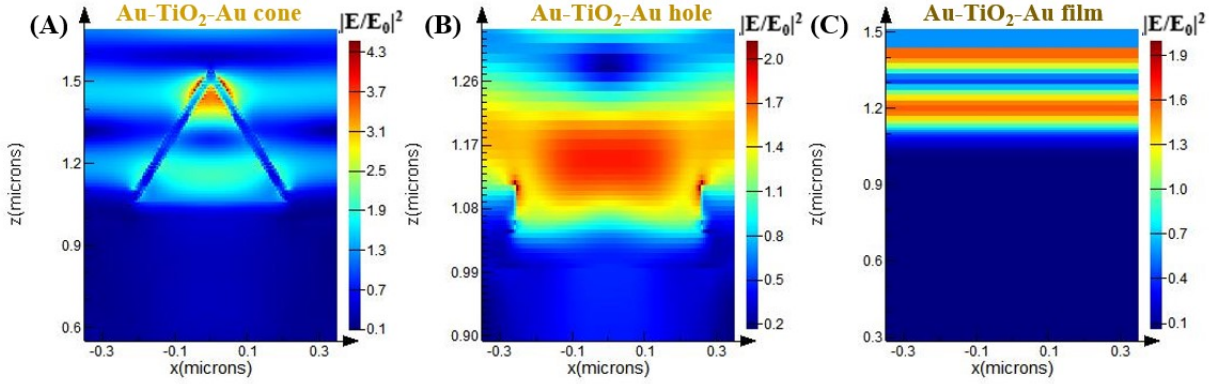

Figure S14. FDTD of Electromagnetic field simulation at 400 nm of (A) Au–TiO_2–Au cone, (B) Au–TiO_2–Au hole, (C) Au–TiO_2–Au film.

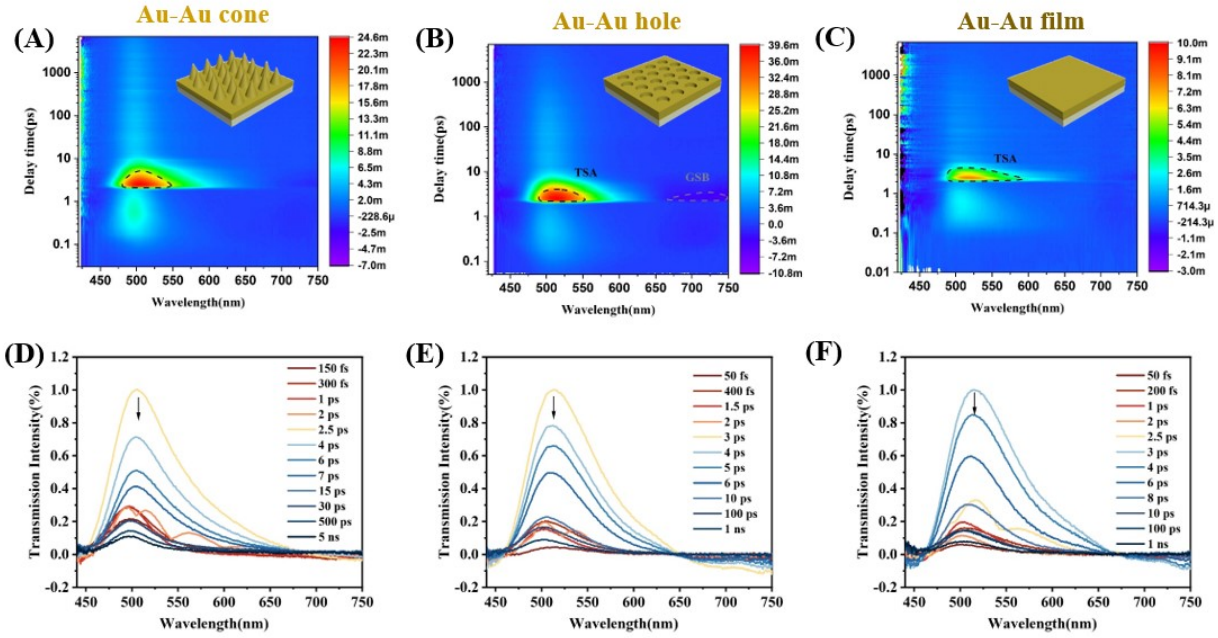

Figure S15. Contour plot of fs-TA spectra of (A) Au–Au cone, (B) Au–Au hole and (C) Au–Au film. TA spectra of (D) Au–Au cone, (E) Au–Au hole and (F) Au–Au film.

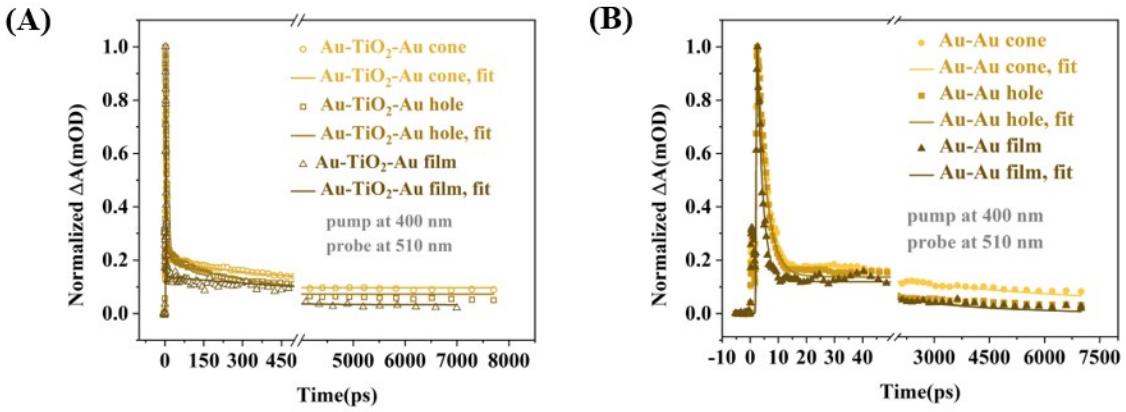

Figure S16. Single-wavelength dynamics of (A) comparison of three heterostructures containing TiO_2 and (B) comparison of three nanostructures without TiO_2. The solid curves are fitting plots.

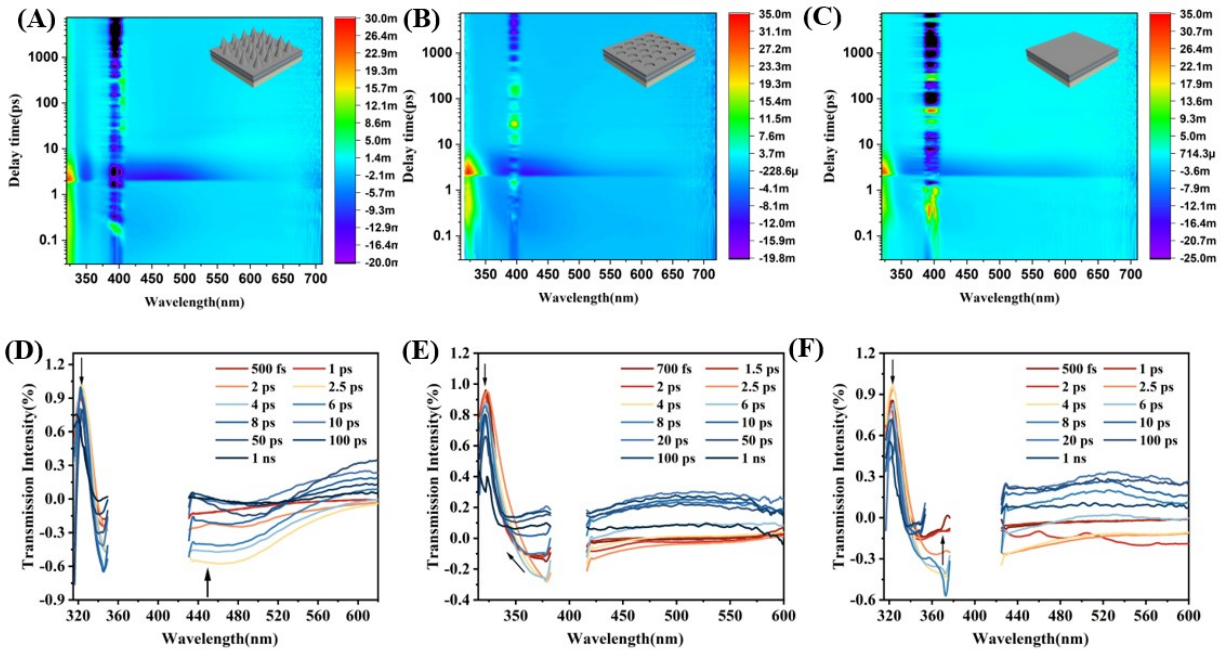

Figure S17. Contour plot of fs-TA spectra of (A) Ag–TiO_2–Ag cone, (B) Ag–TiO_2–Ag hole and (C) Ag–TiO_2–Ag film. TA spectra of (D) Ag–TiO_2–Ag cone, (E) Ag–TiO_2–Ag hole and (F) Ag–TiO_2–Ag film. The spectral discontinuity results from subtracting the 400 nm pump light.

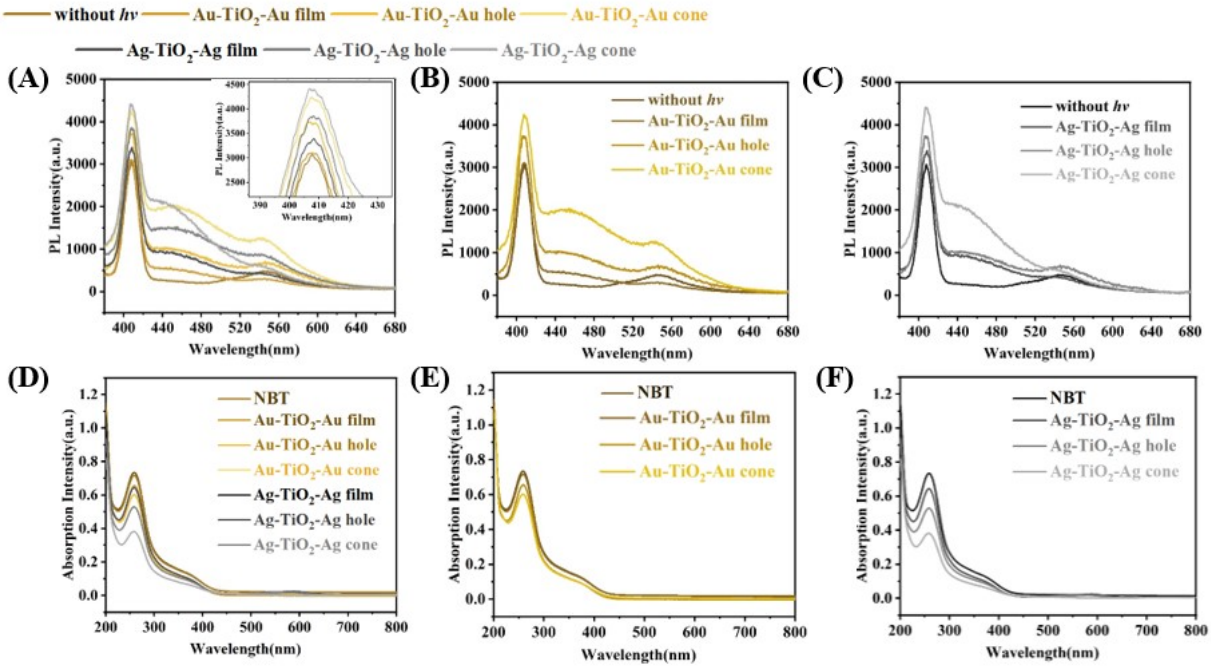

Figure S18. (A-C) Quantitative testing of hydroxyl radicals: fluorescence spectra of six heterogeneous structures after 30-minute irradiation in disodium terephthalate solution. (D-F) Quantitative testing of superoxide radicals: UV-Vis absorption spectra of six heterogeneous structures after 30-minute irradiation in NBT solution.

Table R1. Au-TiO_2-Au peak table after charge correction

Name	Peak BE	Height	CPS FWHM eV	Area (P) CPS.eV	Area (N) TPP-2M	Atomic %
C 1s	284.80	15456.02	1.41	28269.26	0.36	38.59
O 1s	531.40	10065.25	2.77	29403.95	0.14	15.16
Ti 2p	459.55	8475.53	1.11	21353.33	0.04	4.77
Au 4f	83.53	349961.94	0.86	664314.09	0.38	41.48

Table R2. Ag-TiO_2-Ag peak table after charge correction

Name	Peak BE	Height	CPS FWHM eV	Area (P) CPS.eV	Area (N) TPP-2M	Atomic %
C 1s	284.80	32915.85	1.13	46641.32	0.59	52.8
O 1s	530.78	14721.31	1.5	30751.43	0.15	13.15

Ti 2p	458.96	6884.31	1.22	16588.71	0.03	3.07
Ag 3d	368.35	342653.49	0.82	590113.67	0.35	30.98

Table S3. Degradation performance comparison between the photocatalyst reported in this work and various reference photocatalysts.

	Photocatalysts	**Light source**	**Pollutant concentration**	**Reaction time**	**References**
1	Ag-TiO_2 disordered particles	300 W Xe lamps (VIS light)	MB (10 mg L^{-1})	150 min	[51]
2	TiO_2 NPs/Ag NWs	Xe solar simulator (100 mW cm^{-2})	MB (0.05 mm)	150 min	[52]
3	AAO+TiO_2 film +Ag NPs	Laser irradiation (355 nm)	MB (6×10^{-4} M)	180 min	[53]
4	Au+WO_3@TiO_2 Triple-core-shell	300 W Xe lamp	MB (30 ppm)	240min	[54]
5	Ag NPs-TiO_2 NRs nanorods	Natural sunlight	MB (10 μm)	60 min	[55]
6	SiO_2/Ag/SiO_2/TiO_2	150 W Xe lamp ($\lambda > 400$ nm)	MB (10^{-5} M)	175 min	[56]
7	Ag NPs-TiO_2/WO_3 Nanotube film	200 W Xe lamp	MB (2 mg L^{-1})	120 min	[57]
8	**This work**	**300 W Xe lamp**	**MB CV RhB (10^{-5} M)**	**75min**	-